

Measurement of phase fluctuations of Bose-Einstein condensates in an optical lattice

Bing Wang,^{1,2,3} Qiang Zhu,^{1,3} Hailong Zhou,^{1,2,3} Dezhi Xiong,^{1,2} Hongwei Xiong,¹ and Baolong Lü^{1,2,*}

¹State Key Laboratory of Magnetic Resonance and Atomic and Molecular Physics,
Wuhan Institute of Physics and Mathematics, Chinese Academy of Sciences, Wuhan 430071, P. R. China

²Key Laboratory of Atomic Frequency Standards (KLAFS),
Wuhan Institute of Physics and Mathematics, Chinese Academy of Sciences

³Graduate School of the Chinese Academy of Sciences, P. R. China

(Dated: November 20, 2018)

Even at zero temperature, there exist phase fluctuations associated with an array of Bose-Einstein condensates confined in a one-dimensional optical lattice. We demonstrate a method to measure the phase fluctuations based on the Fourier spectrum of the atomic density for a condensate released from the optical lattice. The phase variance is extracted from the relative intensities of different peaks in the Fourier spectrum. This method works even for high lattice strength where interference peaks disappear in the atomic density distribution.

PACS numbers: 03.75.Lm, 67.85.Hj, 37.10.Jk, 67.10.Ba

I. INTRODUCTION

For Bose-Einstein condensates in an optical lattice, the phase fluctuation is a significant quantity in the investigation of quantum phase transitions [1]. The transition from superfluid to Mott insulator is usually accompanied by significantly increased phase fluctuations which can be manifested in the interference pattern of the condensate samples. The vanishing of the contrast of the interference fringes is widely regarded as a characteristic of the quantum phase transition.

The simplest lattice configuration suitable for demonstrating phase fluctuations is a one-dimensional (1D) standing-wave laser field loaded by Bose-Einstein condensates (BEC). Such a 1D optical lattice is actually a common tool to test quantum properties of the cold atoms in periodic potentials. It has been used to demonstrate phase coherence [2, 3], Bloch oscillations [4], number squeezed state [5], Josephson current [6], nonlinear self-trapping of matter waves [7, 8], and so on. In theory, quantum fluctuations in phase and atomic number are often illustrated by considering a BEC in a double-well potential [9–16]. Of course, experimental measurement of the phase fluctuation plays a key role in understanding the quantum process occurring in a lattice.

In a pioneering work by Orzel *et al.* [5], phase fluctuations of the subcondensates in a 1D optical lattice were measured by using the interference pattern of the released condensates. The phase variance was extracted from the contrast of the observed interference peaks. However, at very high lattice depth, the typical interference peaks disappear completely due to the large phase fluctuations, and this method is thus not valid any more. In Ref. [17], it is also shown that, close to the Mott insulator, the vanishing of the interference fringes makes it difficult to describe the quantitative changes of the system controlled

with further increased lattice depth.

In this paper, we develop a method to measure the phase variance by employing the Fourier spectrum of the released atomic cloud. Particularly, a simple analytical expression is found to extract the phase fluctuations. Our method works in principle even when the visibility of the interference peaks is completely lost, as demonstrated in our experiment. It is expected that this method provides a unique tool to other phase transitions in cold atomic systems [18].

The paper is organized as follows. In Sec. II, we present the theoretical model to extract the phase fluctuations from the Fourier spectrum of the atomic density for a condensate released from the optical lattice. In Sec. III, the theoretical model is demonstrated in our experiment. The accuracy and validity of our method are discussed, and a comparison with the method in [5] is also presented. Finally in Sec. IV, we summarize our obtained results.

II. THEORY

We now consider a 1D optical lattice in the dimension of the x axis, formed by a conventional standing-wave laser field. Its strength is usually measured in units of the recoil energy $E_r = h^2/2m\lambda^2$, where m is the atomic mass, h is the Planck constant, and λ the optical wavelength. In the tight-binding limit, the condensate loaded to the lattice can be treated as a chain of disk-shaped subcondensates equally spaced by the lattice period $d = \lambda/2$. The total number of the lattice sites occupied by the condensate is denoted by M . When suddenly released from the optical lattice, the condensate undergoes a free expansion process. After a time of flight (TOF) of τ , the wave function of the atomic cloud can be written as

$$\Psi(x, \tau) = \sum_{l=1}^M \alpha_l \Phi_l(x, \tau),$$

*Electronic address: baolong.lu@wipm.ac.cn

where $\Phi_l(x, \tau)$ refers to the wave function of the subcondensate initially centered at the l th lattice site, and $|\alpha_l|^2$ represents the probability for an atom roughly located at the l th lattice site. The atomic density is then written as

$$\begin{aligned} |\Psi(x, \tau)|^2 &= \sum_{l,q} \alpha_l^* \alpha_q \Phi_l^*(x, \tau) \Phi_q(x, \tau) \\ &= G_0 + \sum_{n=1}^{M-1} G_n, \end{aligned} \quad (1)$$

where G_0 reads

$$G_0 = \sum_{l=1}^M |\alpha_l|^2 |\Phi_l(x, \tau)|^2,$$

while G_n with $n \geq 1$ takes the following form:

$$G_n = \sum_{l=1}^{M-n} \alpha_l^* \alpha_{l+n} \Phi_l^*(x, \tau) \Phi_{l+n}(x, \tau) + \text{c.c.} \quad (2)$$

Note that, G_0 is physically different from other G_n with $n \geq 1$. It contains no interference terms, and is just a direct sum of the atomic densities of all the subcondensates. Therefore, it gives rise to a spatially smooth density profile. In contrast, G_n describes the interference between the subcondensates spaced by nd in the optical lattice. One characteristic associated with G_n must be mentioned. The integration of G_n is zero ($\int G_n dx = 0$) due to the orthogonality between different Φ_l , which implies that G_n would give rise to interference structures rather than a smooth background in the density distribution.

A. Fourier spectrum

According to Eq. (2), the Fourier transform of G_n is

$$\begin{aligned} F_n &= \frac{1}{\sqrt{2\pi}} \sum_l \alpha_l^* \alpha_{l+n} \int \Phi_l^*(x, \tau) \Phi_{l+n}(x, \tau) e^{ikx} dx + \text{c.c.} \\ &= \frac{1}{\sqrt{2\pi}} \tilde{w}_n(k, \tau) \sum_l \alpha_l^* \alpha_{l+n} e^{ikld} + \text{c.c.} \end{aligned} \quad (3)$$

Here,

$$\tilde{w}_n(k, \tau) = \int \Phi^*(x, \tau) \Phi(x - nd, \tau) e^{ikx} dx \quad (4)$$

is independent of the lattice site l . The second line of Eq. (3) is obtained using the fact that all Φ_l are identical wave functions except for their center positions. In the tight-binding limit the Wannier function $\Phi(x, t=0)$ can be well approximated by a Gaussian wave packet $(\pi\sigma^2)^{-1/4} \exp(-x^2/2\sigma^2)$, where $\sigma = \sqrt{\hbar/m\tilde{\omega}_x}$ is the oscillator length, m the atomic mass and $\tilde{\omega}_x/2\pi$ the axial trapping frequency of the lattice wells. After the TOF,

the expanded subcondensate has a much larger size than its initial wave packet ($\hbar\tau/m \gg \sigma^2$), then the wave function of a single subcondensate can be written as [19]

$$\Phi(x, \tau) = \frac{1}{\pi^{1/4} \sigma^{1/2}} \left(1 + \frac{i\hbar\tau}{m\sigma^2} \right)^{-1/2} \exp\left(\frac{imx^2}{2\hbar\tau} \right). \quad (5)$$

Substituting Eq. (5) into Eq. (4), one gets

$$\tilde{w}_n(k, \tau) = W_n \int \exp[ix(k - nk_1)] dx, \quad (6)$$

where $k_1 = 2\pi/\lambda_1$, $\lambda_1 = 2\pi\hbar\tau/dm$ and

$$W_n = \frac{1}{\sqrt{\pi}\sigma} \left| 1 + \frac{i\hbar\tau}{m\sigma^2} \right|^{-1} \exp\left(\frac{in^2md^2}{2\hbar\tau} \right).$$

Here, λ_1 is a characteristic length, equal to the travel distance of an atom with a velocity twice the single photon recoil velocity. The integration term yields a δ -function like peak at $k = nk_1$, and the peak width is inversely proportional to the spatial size of the expanded wave packets. Similar analysis to the conjugate part in F_n yields an identical peak at the symmetric position, $k = -nk_1$, instead. Therefore, the Fourier transform of G_n shows a pair of peaks at $k = \pm nk_1$ (only one peak for G_0). Apparently, the characteristic length λ_1 is actually the spatial period of the Fourier component corresponding to the peak of the $n = 1$ order. As such, coherence properties associated with different spacings between subcondensates in the optical lattice can be distinguished from one another just by inspecting the Fourier spectrum of the density distribution of the expanded atomic cloud. The whole power spectrum of the atomic density is simply given by $S(k) = \sum_n |F_n|^2$.

Note that, λ_1 is much larger than the initial condensate size, which means $kld \ll 1$, and hence $e^{ikld} \simeq 1$. One may get from Eq. (3) the peak intensities in the power spectrum $S(k)$:

$$P_n = |F_n(k = nk_1)|^2 = AY_n, \quad (7)$$

where $A = |\tilde{w}_0(k=0)|^2/2\pi$ and $Y_n = \left| \sum_{l=1}^{M-n} \alpha_l^* \alpha_{l+n} \right|^2$. In particular, $Y_0 = 1$, as required by the normalization condition. From the expression in Eq. (6), one sees that the amplitude of $\tilde{w}_n(k = nk_1)$, and hence A , is independent of n . Therefore, the relative intensity of peaks in the power spectrum depends only upon Y_n .

B. Phase Fluctuations

We now turn to consider the peak intensities in the power spectrum, from which the phase fluctuation can be deduced. In the optical lattice, the confined subcondensates undergo phase fluctuations. The phase factor of each subcondensate is contained in the corresponding

coefficient α_l , and the summation term Y_n in Eq. (7) is then rewritten as

$$Y_n = \left| \sum_{l=1}^{M-n} |\alpha_l \alpha_{l+n}| e^{i\phi_{ln}} \right|^2 \\ \simeq \left(\sum_l |\alpha_l \alpha_{l+n}| \right)^2 \left| \frac{1}{M-n} \sum_l e^{i\delta\phi_{ln}} \right|^2,$$

where $\delta\phi_{ln} \equiv \phi_{l+n} - \phi_l$. Due to phase fluctuations of the subcondensates when trapped in the optical lattice, $\delta\phi_{ln}$ takes random values with zero average. The last line of the above equation is obtained by assuming that $|\alpha_l \alpha_{l+n}|$ changes slowly with l . As long as $n \ll M$, the summation term $\sum_l |\alpha_l \alpha_{l+n}|$ is constant for different n , i.e., $\sum_l |\alpha_l \alpha_{l+n}| \simeq \sum_l |\alpha_l|^2 = 1$. Y_n is then simplified to:

$$Y_n = \left| \frac{1}{M-n} \sum_l e^{i\delta\phi_{ln}} \right|^2. \quad (8)$$

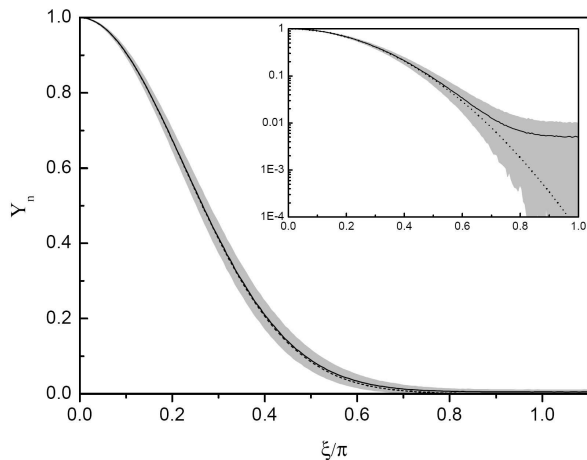


FIG. 1: The solid line shows the numerically calculated Y_n versus the variance of the random phase $\delta\phi_{ln}$ for a total lattice number $M = 200$. Each data point is an average of 1000 individual runs of the computation. Shaded area corresponds to the standard error. The dashed line is an exponential curve in the form of $e^{-\xi^2}$. The inset is the same figure on a logarithm vertical scale, highlighting the discrepancy between the two curves.

Apparently, for $n > 0$, Y_n depends on the variance of $\delta\phi_{ln}$, denoted by $\xi^2 = \langle \delta\phi_{ln}^2 \rangle$. As shown in Fig. 1, Y_n drops quickly with increasing ξ . The randomness of $\delta\phi_{ln}$ results in the fluctuations of Y_n around its averaged values. In the region of larger phase variance, Y_n has larger fractional fluctuations. In computation, the total lattice site number is assumed to be $M = 200$. We find, however, the averaged value of Y_n is nearly unchanged for different values of M .

Checking the summation $\sum_l e^{i\delta\phi_{ln}}$ in Eq. (8), one sees that it is nearly a real number as the imaginary terms are

averaged to zero. By replacing $\delta\phi_{ln}$ by its variance ξ and assuming $\xi \ll 1$, this summation term can be approximated by $(M-n)e^{-\frac{1}{2}\xi^2}$. We then have an approximated expression of Y_n in an exponential form:

$$Y_n = e^{-\xi^2}. \quad (9)$$

This exponential curve is plotted in Fig. 1 as well. Surprisingly, it shows a good match to the numerical data (the solid curve in Fig. 1) even for the region far beyond $\xi \ll 1$. For example, the relative error is only 5% at $\xi = 0.5\pi$. Of course, the tendency to larger relative errors can be clearly seen as ξ is increased.

The phase fluctuation of two adjacent subcondensates can be measured by a phase variance $\sigma^2 = \langle \delta\phi_{l1}^2 \rangle$. It is straightforward to prove that two subcondensates spaced by n times the lattice period correspond to a n times larger phase variance, i.e., $\xi^2 = n\sigma^2$. One knows from Eq. (7) and (9) that $P_n = Ae^{-n\sigma^2}$. Taking natural logarithm for both sides of this formula, one obtains

$$\ln P_n = \ln A - n\sigma^2, \quad (10)$$

which clearly shows the linear relation between the logarithmic scale of the peak height and subcondensate spacing n . The slope of this linear curve is just the phase variance σ^2 . Therefore, the phase fluctuations of the condensates confined in discrete lattice wells can be easily determined by the peak structures in the Fourier spectrum of the atomic density distribution after the time of flight. We stress here that this method to measure σ^2 does not need exact calibration of the peak intensities, because σ^2 is unaffected by any identical scale factors applied to all P_n . This clearly shows the convenience of Eq. (10) in the measurement of σ^2 .

There also exists an alternative method to measure the phase variance, where σ^2 is determined by comparing the experimentally measured P_n with numerically calculated Y_n . When ξ is very large, the analytical expression of Y_n in Eq. (9) is not a good approximation any more. In this case, the second method is more reliable than the former one based on Eq. (10). We shall make a comparison between the two methods later.

III. EXPERIMENT

Our experiments are carried out by using a nearly pure ^{87}Rb condensate in the hyperfine state $|F = 2, M_F = 2\rangle$ with typically 10^5 atoms. The experimental setup was described elsewhere [19]. The 1D optical lattice is formed by a retroreflected laser beam with a wavelength of $\lambda = 1064$ nm. Its strength is calibrated using a method of Kapitza-Dirac scattering [17, 20]. The recoil energy is $E_r = h \times 2.03$ kHz. The lattice light is adiabatically applied to the cigar-shaped condensate along its axial direction during a time of 50 ms. After a holding time of 10 ms, the lattice light, as well as the magnetic trap, are suddenly switched off. Finally, an absorption image is

taken for the released atomic cloud after a 30 ms of TOF, by using a probe light directed perpendicular to the lattice beam. The experimental parameters correspond to a characteristic length $\lambda_1 = 259 \mu\text{m}$, which is much larger than the pixel size ($9 \mu\text{m}$) of our CCD camera. In principle, the peaks up to the order of $n = 14$ can be resolved by the CCD camera. In order to obtain the statistics of the phase variance, the experiment was repeated at least eleven times for each lattice depth.

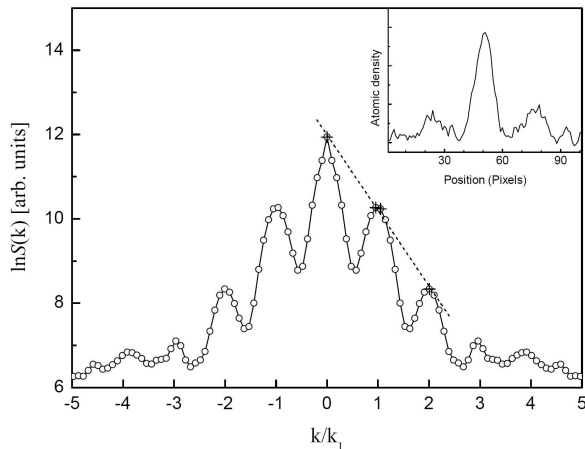


FIG. 2: Open circles show the power spectral intensity obtained from the density distribution of an expanded condensate released from an optical lattice with a depth of $34.6 E_r$. Four points at the top of three peaks are marked by crosses, and used to determine a phase variance of $\sigma^2 = 1.79(8)$ by a linear fit (dashed line). The peak close to $k/k_1 = 3$ is caused by optical noises of the probe light. The inset shows the atomic density distribution of this atomic cloud along the direction of the lattice beam, showing clearly two side peaks due to the interference of the subcondensates.

The power spectrum $S(k)$ is obtained from an absorption image as follows: Spatial frequency spectrum is calculated by Fourier-transforming the matrix of image. Taking the absolute square to obtain the 2D power spectral density, and $S(k)$ is then obtained from the 2D matrix by making summation along the direction perpendicular to the lattice beam. Thus, only the power spectrum along the lattice direction is remained in $S(k)$. Finally, taking the natural logarithm of $S(k)$, we can find the peaks and extract σ^2 according to Eq. (10).

Figure 2 displays a power spectrum corresponding to the absorption image of an atomic cloud released from the optical lattice with a depth of $34.6 E_r$. As predicted, $S(k)$ consists of a series of peaks equally spaced by k_1 . The peaks with $n = 0-2$ are true signals of the cold atoms, whereas the peak close to $k/k_1 = 3$ is confirmed to be optical noise of the probe light itself. This noise peak appears occasionally in repeated experiments, even in the absence of the atomic cloud.

A higher phase variance means a weaker phase correlation. In our experiment, subcondensate pairs with a spacing larger than $2d$ can not yield a peak ($n > 2$) high

enough to be visible in $S(k)$. We thus inferred that the phase correlation of two subcondensates drops quickly with increased distance between them, which is a natural consequence of the proportional relation of $\xi^2 = n\sigma^2$.

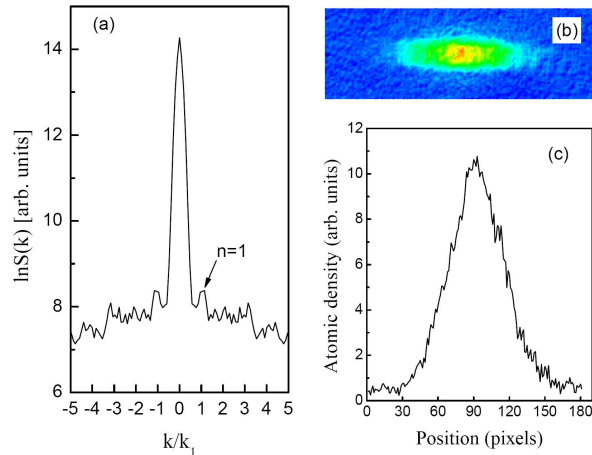


FIG. 3: (Color online) (a) Power spectrum $S(k)$ of an expanded condensate initially trapped at a depth of $68 E_r$. (b) A false-color absorption image of this released condensate, with a field of view of $0.55 \text{ mm} \times 1.63 \text{ mm}$. (c) Atomic density in the x direction, which is obtained by integrating the pixels in height.

To extract the phase variance σ^2 , we used the data points at the top of peaks in a power spectrum to perform the linear fit in the form of Eq. (10). The standard error of a fitted slope (σ^2) is usually small ($\leq 5\%$). In contrast, the value of σ^2 shows much larger fluctuations from shot to shot as the experiment is repeated under the same conditions. We thus take only the latter fluctuations into consideration when calculating the error bars of the phase variance. A linear fit to the three peaks in Fig. 2 yields a phase variance of $\sigma^2 \simeq 1.79$. At the corresponding depth level of the optical lattice, the atomic density profile exhibits clear interference peaks along the lattice direction (see the inset in Fig. 2). As the lattice depth is increased, the phase variance is increased, and the higher order peaks in $S(k)$ with $n \geq 1$ are expected to become weaker accordingly. Figure 3 displays a typical result in such a case. At the depth of $68 E_r$, only the peaks of $n = 0, 1$ are observed. Higher order peaks are too weak to be identified. As seen from Fig. 3 (b) and (c), the released condensate has lost the interference structures completely, in contrast to the side peaks in Fig. 2. In fact, despite the loss of interference peaks in atomic density distribution, the peaks in $S(k)$ can still be observed for strong optical lattice, up to the highest level ($120 E_r$) we have reached.

The dependence of phase variance σ upon the lattice depth is displayed in Fig. 4. The two sets of data (blue and red ones) were obtained using the two methods described in Sec. II B. There exists a clear trend, where the deeper the optical lattice, the larger the phase variance.

The value of σ grows from $\sim 0.4\pi$ to $\sim \pi$, indicating that the relative phase between adjacent lattice sites gains increased randomness, and tend to be a completely random phase. Below $50 E_r$, the blue data points are very close to the red ones. Beyond this level, however, the discrepancy between the two sets of data becomes larger with increased lattice depth. It can be simply understood by the fact that the exponential form of Y_n (Eq. (9)) is not a good approximation for large ξ . Roughly speaking, the linear fit method can only be applied when ξ is less than 0.6π , as is evident in Fig. 4. It is worthy to point out that, although the linear fit method is invalid in this case, the alternative method is still simple to extract the phase variance from the Fourier spectrum.

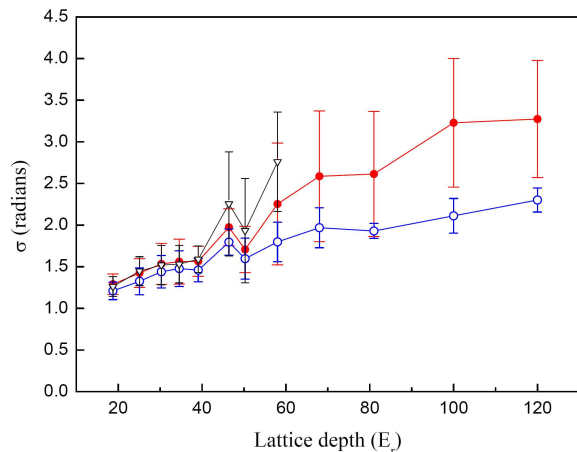


FIG. 4: (Color online) Measured phase variance σ versus the lattice depth. For each data point, eleven independent runs were averaged. Blue data points were obtained based on Eq. (10), whereas, the red data points were obtained by comparing the measured relative intensity of the peaks of $n = 1$ with the numerical values of Y_1 . Black data points were obtained by fitting the atomic density profile using the method in [5].

The accuracy of phase variance σ is limited by at least two factors. First, as shown by the solid curve in Fig. 1, Y_n is less sensitive to ξ when ξ becomes large, particularly in a region around π . Second, Y_n itself is in fact a fluctuating parameter in principle, although we have taken its averaged value as the measured result. The fluctuation is evident from the fact that the relative intensity of each peak in $S(k)$ varies from shot to shot. Therefore, in the deep lattice region, data points of σ are always accompanied by large error bars.

As a comparison, we have also extracted the phase variance by analyzing the visibility of the interference peaks of the released atomic cloud. This method was first demonstrated in [5], where the visibility is characterized by a quantity ζ defined as the ratio of the width of a single peak to separation between the peaks. The phase variance is determined by comparing the observed value of ζ with those obtained from simulated data sets. First, we fit the interference profile with three Gaussian

peaks to get the value of ζ . Then, we calculate the interference profile by using a simple one-dimension model which is similar to that in our previous work [19]. Each subcondensate in a single lattice well is assigned a random phase. Those random phases are set in such a way that the phase difference between two adjacent lattice sites obeys a Gaussian distribution with a given variance σ^2 . We convolve the calculated interference profile with a resolution function to account for the limited resolution of our imaging system. To obtain the simulated ζ , we fit the convolved waveform with the same fit function applied to the experimental data. The simulation procedure is repeated many times to obtain an averaged value of the simulated ζ .

The phase variances deduced from this fitting method are displayed in figure 4. It is obvious that, below a depth level of $\sim 60 E_r$, the results of the fitting method agree well with our method. This further confirms the validity of our method. However, above $60 E_r$, the fitting method does not work due to the following reasons: To strictly follow the method demonstrated in [5], both the peak width and peak separation must be treated as fitting parameters. However, at high lattice-depth level, only one broad peak is left in the interference profile, as shown in Fig. 3(c). The fitting procedure cannot give reasonable peak positions. More specifically, the side peaks obtained from the fitting program deviate significantly from the positions where they should be located. In addition, the fitted width of the side peaks is not reliable.

IV. SUMMARY AND DISCUSSION

We have developed a method to measure the phase fluctuations of the subcondensates confined in a 1D optical lattice. In our method, the Fourier spectra of the conventional absorption images of the released atomic clouds have been investigated. The phase variance between adjacent lattice wells is deduced from the relative intensities of the peaks in a Fourier power spectrum. Our experimental measurements have displayed an increased phase variance as the lattice depth becomes larger, and also indicated that phase correlation of two lattice wells decreases quickly with the increased distance between them. Our method does not rely on the existence of interference peaks of the released condensates, and it works even for very large lattice depth. This method is a complementary to that demonstrated in [5], and will be a useful tool in analyzing phenomena associated to phase fluctuations in optical lattice systems, particularly for the case close to the quantum phase transition.

Our theoretical model is established in the tight-binding limit, where a condensate in the optical lattice can be regarded as a chain of subcondensates. We found that, for weak optical lattice, there is no multi-peak structure in $S(k)$. The peaks start to appear when the lattice depth reaches a level of $\sim 10 E_r$. Well resolved peaks can be observed if the depth level is further

increased to $\sim 20 E_r$. It sets a coarse boundary beyond which our model is applicable. Below the level of $20 E_r$, one has to switch to the method in [5] to measure the phase variance.

The optical lattice is not homogeneous due to the presence of the magnetic trap which is used to support the atoms against the gravity. The harmonic confinement of the magnetic trap corresponds to a trapping frequency of $2\pi \times 7.6$ Hz, and it remains until the sudden release of the atomic cloud. For a total atomic number of 10^5 , the number of lattice sites that are populated is $M \simeq 200$. Most atoms are distributed in the center region of the lattice where the tunneling rate J is nearly uniform. This assures the assumption that σ is uniform over the optical lattice. On the other hand, we did not see noticeable changes of σ as the total atomic number is changed from $4 - 15 \times 10^4$. It is due to the fact that the tunneling rate is independent of the atom numbers in single lattice

wells.

In principle, our method can be extended to 2D and 3D optical lattices by treating the power spectrum in each dimension separately. For a 2D optical lattice, one probe beam perpendicular to the lattice plane is enough. For a 3D lattice, however, an additional probe beam is required to detect the atomic density profile in the third dimension.

Acknowledgments

This work is supported by the National Natural Science Foundation of China under Grant Nos. 11174331, 11175246 and 11104322, and by the National Key Basic Research and Development Program of China under Grant No. 2011CB921503.

-
- [1] M. Greiner, O. Mandel, T. Esslinger, T. W. Hänsch, and I. Bloch, *Nature* **415**, 39 (2002).
 - [2] P. Pedri, L. Pitaevskii, S. Stringari, C. Fort, S. Burger, F. S. Cataliotti, P. Maddaloni, F. Minardi, and M. Inguscio, *Phys. Rev. Lett.* **87**, 220401 (2001).
 - [3] X. Zhou, X. Xu, L. Yin, W. Liu, and X. Chen, *Optics Express* **18**, 15664 (2010).
 - [4] E. Peik, M. B. Dahan, I. Bouchoule, Y. Castin, and C. Salomon, *Phys. Rev. A* **55**, 2989 (1997).
 - [5] C. Orzel, A. K. Tuchman, M. L. Fenselau, M. Yasuda, and M. A. Kasevich, *Science* **291**, 2386 (2001).
 - [6] F. S. Cataliotti, S. Burger, C. Fort, P. Maddaloni, F. Minardi, A. Trombettoni, A. Smerzi, and M. Inguscio, *Science* **293**, 843 (2001).
 - [7] Th. Anker, M. Albiez, R. Gati, S. Hunsmann, B. Eiermann, A. Trombettoni, and M. K. Oberthaler, *Phys. Rev. Lett.* **94**, 020403 (2005).
 - [8] B. Wang, P. Fu, J. Liu, and B. Wu, *Phys. Rev. A* **74**, 063610 (2006).
 - [9] M. W. Jack, M. J. Collett, and D. F. Walls, *Phys. Rev. A* **54**, R4625 (1996).
 - [10] G. J. Milburn, J. Corney, E. M. Wright, and D. F. Walls, *Phys. Rev. A* **55**, 4318 (1997).
 - [11] J. Javanainen and M. Wilkens, *Phys. Rev. Lett.* **78**, 4675 (1997).
 - [12] K. Molmer, *Phys. Rev. A* **58**, 566 (1998).
 - [13] J. Javanainen, and M. Y. Ivanov, *Phys. Rev. A* **60**, 2351 (1999).
 - [14] A. J. Leggett and F. Sols, *Found. Phys.* **21**, 353 (1991).
 - [15] F. Sols, *Physica B: Condensed Matter* **194-196**, 1389 (1994).
 - [16] I. Zapata, F. Sols, and A. J. Leggett, *Phys. Rev. A* **57**, R28 (1998).
 - [17] R. E. Sapiro, R. Zhang, and G. Raithel, *New J. Phys.* **11**, 013013 (2009).
 - [18] I. Bloch, J. Dalibard, and W. Zwerger, *Rev. Mod. Phys.* **80**, 885 (2008).
 - [19] B. Lü, X. Tan, B. Wang, L. Cao, and H. Xiong, *Phys. Rev. A* **82**, 053629 (2010).
 - [20] D. L. Freimund, K. Aflatooni, and H. Batelaan, *Nature* **413**, 142 (2001).